Title

Glutathione deficiency decreases lipid droplet stores and increases reactive oxygen species in mouse oocytes†

Journal

Biology of Reproduction, 106(6)

ISSN

0006-3363

Authors

Malott, Kelli F

Reshel, Samantha

Ortiz, Laura

et al.

Publication Date

2022-06-13

DOI

10.1093/biolre/ioac032

Peer reviewed

Biology of Reproduction, 2022, **106(6)**, 1218–1231
https://doi.org/10.1093/biolre/ioac032
Advance access publication date 3 March 2022
Research Article

Glutathione deficiency decreases lipid droplet stores and increases reactive oxygen species in mouse oocytes†

Kelli F Malott[1,2,3], Samantha Reshel[4], Laura Ortiz[3] and Ulrike Luderer[1,2,3,4,*]

[1]Environmental Health Sciences Graduate Program, University of California, Irvine, CA, USA
[2]Department of Environmental and Occupational Health, University of California, Irvine, CA, USA
[3]Department of Medicine, University of California, Irvine, CA, USA
[4]Department of Developmental and Cell Biology, University of California, Irvine, CA, USA

***Correspondence**: Center for Occupational and Environmental Health, 100 Theory Drive, Suite 100, Irvine, CA 92617, USA. Tel: +19498248641; E-mail: uluderer@uci.edu

†**Grant Support**: National Institutes of Health (NIH) R01ES020454 and R21HD097541 to UL. Tobacco Related Diseases Research Program Predoctoral Fellowship T30DT0816 to KFM. The authors wish to acknowledge the support of the UC Irvine Chao Family Comprehensive Cancer Center Optical Biology Shared Resource, supported by the National Cancer Institute of the NIH under award number P30CA062203. West Coast Metabolomics Center, University of California, Davis, supported by National Institutes of Health U2CES030158.
The content is solely the responsibility of the authors and does not necessarily represent the official views of the National Institutes of Health.

Abstract

Glutathione (GSH) is a tripeptide thiol antioxidant that has been shown to be important to overall reproductive health. Glutamate cysteine ligase, the rate-limiting enzyme in GSH synthesis consists of a catalytic and a modifier (GCLM) subunit. We previously showed that oxidative stress in the ovary and oocytes of *Gclm*$^{-/-}$ mice is associated with accelerated age-related decline in ovarian follicles and decreased female fertility due to preimplantation embryonic mortality. Mammalian preimplantation development is a highly regulated and energy-intensive process that primarily relies on coordination between lipid droplets (LDs) and mitochondria to maintain cellular homeostasis. In this study, we hypothesized that GSH deficiency in oocytes increases oxidative stress, leading to increased mitochondrial dysfunction and decreased LD consumption, thereby decreasing oocyte developmental competence. We observed that *Gclm*$^{-/-}$ oocytes have increased oxidative stress, primarily in the form of mitochondrial superoxide and decreased subcortical mitochondrial clusters. Further, *Gclm*$^{-/-}$ oocytes have decreased mitochondrial membrane potential ($\Delta\Psi$m) compared with *Gclm*$^{+/+}$. We surmise this is likely due to the decreased availability of LDs, as we observed a significant decrease in LD content in *Gclm*$^{-/-}$ oocytes compared with *Gclm*$^{+/+}$. The decreased oocyte LD content is likely related to an altered serum lipidome, with *Gclm*$^{-/-}$ serum having relatively lower unsaturated fatty acids and triglycerides than that of *Gclm*$^{+/+}$ and *Gclm*$^{+/-}$ females. Altogether these data support that decreased LDs and increased oxidative stress are primary drivers of decreased oocyte developmental competence in GSH-deficient oocytes.

Summary Sentence

Glutathione deficiency leads to increased oocyte oxidative stress, reduced mitochondrial membrane potential, and aberrant lipid storage, reducing oocyte competence.

Received: August 30, 2021. **Revised:** January 6, 2022. **Accepted:** February 1, 2022

Graphical Abstract

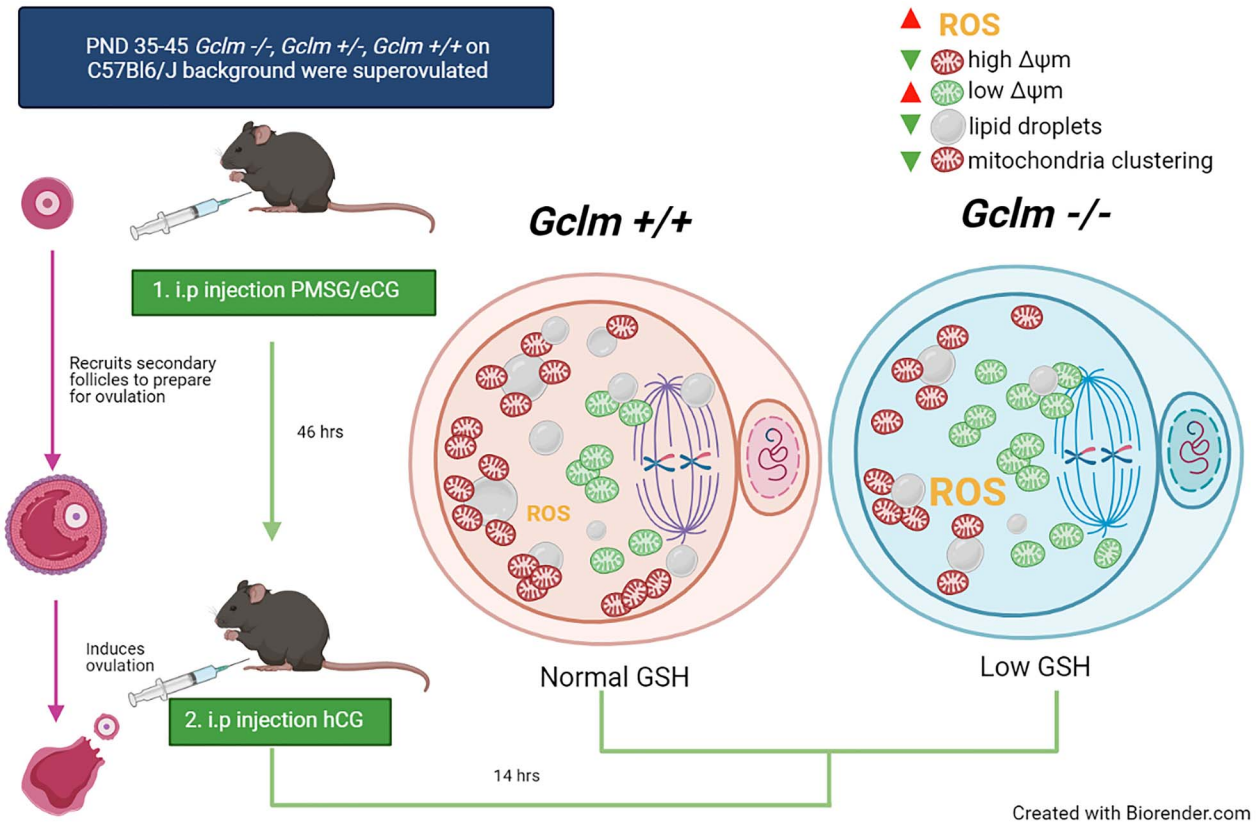

Keywords: oocyte, mitochondria, lipid droplets, glutathione, oxidative stress, lipidomics

Introduction

Glutathione (GSH) is an important tripeptide and thiol antioxidant that is produced through two ATP-dependent reactions. The first, mediated by the enzyme glutamate cysteine ligase (GCL), is the rate-limiting reaction [1]. GCL is composed of two subunits, the catalytic and modifier subunits, GCLC and GCLM, respectively [2]. Deletion of *Gclc* is embryonic lethal [3]. $Gclm^{-/-}$ mice, however, have apparently normal lifespans despite tissue GSH concentrations that are about 75–90% lower than levels in $Gclm^{+/+}$ mice [4–7].

Mammalian preimplantation development is a highly regulated process that requires oocyte developmental competence, as the preimplantation embryo relies almost entirely on the oocyte for successful development [8]. The mature oocyte has among the highest GSH concentrations of any cell type, around 10 mM [9, 10]. GSH stores in the oocyte have been shown to be important for sperm nuclear decondensation, male pronuclear formation, and the formation of the meiotic spindle during meiosis II [9–12]. Previously, we observed that female $Gclm^{-/-}$ and $Gclm^{+/+}$ mice produced equal numbers of litters, but the $Gclm^{-/-}$ females produced significantly fewer pups [5]. The decreased offspring production was not caused by increased postimplantation death, as no increases in uterine resorption sites or number of dead fetuses were observed [5]. Instead, we observed increased preimplantation mortality. Oocytes and conceptuses derived from $Gclm^{-/-}$ females progressed to the two pronuclei stage and to the blastocyst stage in vivo and in vitro at much lower rates than conceptuses from $Gclm^{+/-}$ and $Gclm^{+/+}$ females [5]. These data taken together show that the normally high oocyte GSH concentration is important to preimplantation development. Further, we have previously demonstrated that $Gclm^{-/-}$ ovaries undergo increased oxidative stress in the form of increased lipid peroxidation marker, 4-hydroxynonenal (4-HNE), and increased protein oxidative damage marker nitrotyrosine, in both pubertal and adult ovaries compared with $Gclm^{+/+}$ [13]. Prepubertal $Gclm^{-/-}$ ovaries displayed increased percentages of transitional/primary follicles with mitotic granulosa cells, suggesting increased recruitment into the growing follicle pool. These data combined with the observation of accelerated age-related decline in ovarian follicle numbers in $Gclm^{-/-}$ compared with $Gclm^{+/+}$ mice all suggest that GSH is an important antioxidant for maintaining a healthy ovarian reserve and preventing accelerated age-related ovarian failure [13]. Left unaddressed in these inquiries was how GSH deficiency alters oocyte developmental competence in the mature MII oocyte.

Oogenesis is the progressive process through which the female germ cell acquires the ability to successfully complete meiosis, ensure monospermic fertilization, decondense the sperm head, and undergo preimplantation development [14, 15]. This developmental competence is achieved through nuclear maturation, including nuclear envelope breakdown, meiotic spindle formation, and first polar body extrusion

upon ovulation [16]; and cytoplasmic maturation, including stockpiling organelles such as endoplasmic reticula, mitochondria, and lipid droplets (LDs), as well as small molecules such as mRNA, ATP, and GSH [16].

Mitochondria are among the most abundant organelles in a healthy, mature oocyte, with each murine oocyte possessing roughly 100 000 mitochondria [17–20]. It is hypothesized that oocyte mitochondria are maintained in a less active state [21] to reduce reactive oxygen species (ROS) production by active oxidative phosphorylation while still supplying enough ATP to meet the needs of the oocyte, primarily through pyruvate oxidation up until ovulation [22–24]. Mitochondria are the primary source of ROS in cells, converting 0.2–2% oxygen taken up by the oocyte into ROS [25]. Proteins along the electron transport chain partially reduce molecular oxygen, producing the highly reactive superoxide anion radical ($O_{2-}^{\bullet}$), which is readily converted to hydrogen peroxide and other ROS [17, 25]. ROS are well characterized cell signaling molecules, but in excess, ROS can shift the redox state of the cell causing oxidative stress [14, 17, 26].

Lipid droplets (LDs) are ubiquitous organelles, composed of a neutral, primarily, triacylglycerol core enclosed in a monophospholipid layer [27, 28]. Oocytes possess LDs that are composed of triacylglycerols formed from free fatty acids taken up from the follicular fluid, supplied through the blood serum [17, 29]. Triacylglycerols and free fatty acids are present in the follicular fluid of several mammalian species, including mice and humans [29, 30]. Lipids in the oocyte can be taken up from the follicular fluid or broken down from endogenous cellular lipid to be stored in LDs [14]. LDs are multifaceted organelles that supply secondary signaling molecules [27, 31], supply phospholipids for cellular membrane maintenance [28, 31], and provide lipoic acid, an important cofactor for mitochondrial dehydrogenases, that generate NADH to regulate cellular homeostasis [32]. LDs and mitochondria have been demonstrated to colocalize in porcine oocytes using fluorescence resonance energy transfer [33]. Triacylglycerol stored within oocyte LDs can also be hydrolyzed by lipases to provide free fatty acids for mitochondrial fatty acid β-oxidation, which is required for oocyte nuclear maturation and developmental competence [30, 34, 35]. Inhibition of mitochondrial fatty acid uptake by the carnitine palmitoyl transferase I inhibitor etomoxir hindered mouse oocyte maturation and reduced the rate of blastocyst formation [36, 37]. Moreover, delipidated MII oocytes will expend precious resources to rebuild LDs through de novo lipogenesis to support fertilization [38].

In the current study, we used our *Gclm*$^{-/-}$ mouse model to explore the effects of low oocyte GSH concentrations on oocyte quality. We hypothesized that oocytes derived from *Gclm*$^{-/-}$ females have increased ROS levels due to low GSH concentrations, which results in mitochondrial dysfunction, lipid oxidation, and telomere shortening, a hallmark of aging. We further hypothesized that oocytes from *Gclm*$^{-/-}$ females contain fewer LDs.

Materials and methods

Animals

Gclm null mice were generated by disrupting the *Gclm* gene by replacing exon 1 with a beta-galactosidase/neomycin phospho-transferase fusion minigene [5, 7]. The mice had been backcrossed 10 times onto a C57BL/6J genetic background (B6.129-*Gclm*^{tm1Tjka}; hereafter referred to as *Gclm*$^{-/-}$). Mice for these experiments were generated at the University of California Irvine (UC Irvine) and housed in an American Association for the Accreditation of Laboratory Animal Care-accredited facility, with free access to deionized water and soy-free laboratory chow (Harlan Teklad 2919) on a 14:10 h light–dark cycle. Offspring were genotyped by Transnetyx (Cordova, TN) by PCR using primers for both the native *Gclm* sequence and the β-Geo sequence on DNA extracted from toe snips as previously described [5]. Temperature was maintained at 21–23°C. The experimental protocols were carried out in accordance with the Guide for the Care and Use of Laboratory Animals [39] and were approved by the Institutional Animal Care and Use Committee at UC Irvine.

Superovulation

Postnatal day (PND) 35–45 *Gclm*$^{+/+}$, *Gclm*$^{+/-}$, and *Gclm*$^{-/-}$ females were primed to produce a large cohort of preovulatory follicles by i.p. injection with 5 IU equine chorionic gonadotropin (eCG) (Prospec Protein Specialists, Israel) at 18:00 h; 46 h later ovulation was induced by an i.p. injection with 5 IU human chorionic gonadotropin (hCG) (Sigma Aldrich, St. Louis, MO). Then, after 12–14 h, cumulus–oocyte complexes were harvested, following CO_2 euthanasia, from the ampullae of the oviducts into flushing and holding medium (FHM) (Neta Scientific, Hainesport, NJ). Oocytes were dissociated from the cumulus clouds by incubation in 0.3 mg/mL hyaluronidase (Thermo Fisher Scientific) for no more than 5 min, then immediately transferred to FHM under mineral oil (Sigma-Aldrich, St. Louis, MO) for assessment. Morphologically healthy oocytes were defined as having clear, granular cytoplasm; small perivitelline space; first polar body; colorless zona pellucida; and not fragmented. For the following experiments, one *Gclm*$^{-/-}$ female and age-matched *Gclm*$^{+/+}$ and/or *Gclm*$^{+/-}$ female were superovulated at the same time per experimental replicate.

Measurement of reactive oxygen species

To measure oocyte ROS levels, 2–3 morphologically healthy oocytes from *Gclm*$^{-/-}$ and *Gclm*$^{+/+}$ females per experimental replicate were incubated in 10 μM H_2-DCFDA (2′,7′-dichlorofluorescin diacetate) (Thermo Fisher Scientific, Waltham, MA) in FHM under mineral oil at 37°C and 5% CO_2 for 15 min. Two oocytes from each genotype were incubated with 0.003% hydrogen peroxide plus H_2-DCFDA as positive control oocytes and two oocytes from each genotype were incubated with FHM alone as negative controls. Upon entering the cell, H_2-DCFDA is deacetylated by cellular esterases, yielding a nonfluorescent compound, which is oxidized by ROS into a highly fluorescent compound. Oocytes were then washed through three droplets of FHM under mineral oil and imaged in a glass-bottomed petri dish in 50-μL droplets of FHM without phenol red under mineral oil. Oocytes were imaged using a Zeiss Axiovert 200 M microscope (Zeiss, Oberkochen, Germany) at 40× objective with FITC excitation. Images were captured using an Axiovision camera, and fluorescence intensity was quantified using the ImageJ software to estimate levels of ROS. Specifically, the corrected total cell fluorescence (CTCF) was obtained by subtracting the product of area of the selected cell and the fluorescence of background measurements from the integrated density of the selected oocyte (CTCF = integrated

density – [area of selected cell × background fluorescence]) [40]. On every experimental day, oocytes from *Gclm*$^{-/-}$ and *Gclm*$^{+/+}$ mice were imaged, and the fluorescence intensity for each experimental oocyte of each genotype was expressed as the number of times the average fluorescence in the respective positive control oocytes from the same experimental day. This allowed for normalization across experimental days.

Measurement of neutral and oxidized lipid droplets

To measure the ratio of oxidized:unoxidized lipids, 2–3 morphologically healthy oocytes per genotype per experimental replicate were incubated in 10 μM BODIPY 581/591 C11 (Thermo Fisher Scientific, D3861) at 37°C and 5% CO_2 for 30 min under mineral oil, then washed through three droplets of FHM. Oocytes were imaged in glass-bottomed petri dishes in 50-μL droplets of FHM without phenol red under mineral oil. BODIPY 581/591 C11 colocalizes with fatty acids inside the cell; upon oxidation of the polyunsaturated butadienyl portion, the fluorescence emissions peak shifts from ∼590 to ∼510 nm, this red-to-green fluorescence shift allows for the use of green:red ratio reporting of oxidized lipids.

To measure the total neutral lipid content, 2–3 morphologically healthy oocytes per genotype per experimental replicate were fixed with 4% paraformaldehyde for 1 h at room temperature, then washed through three droplets of 1× phosphate-buffered saline (PBS) with 3 mg/mL polyvinylpropylene (PVP) (Thermo Fisher Scientific, P0930). Fixed oocytes were incubated in 3.82 μM BODIPY 493/503 (4,4-difluoro-1,3,5,7,8-pentamethyl-4-bora-3a,4a-diaz-s-indacene) (Thermo Fisher Scientific, D3922) for 1 h at room temperature under mineral oil, washed through three droplets of 1× PBS with 3 mg/mL PVP then imaged in glass-bottomed petri dishes in 50-μL droplets of 1× PBS under mineral oil. BODIPY 493/503 is a nonpolar lipid stain. Total lipid droplet content per oocyte was estimated by the sum fluorescence per cell.

Measurement of mitochondrial membrane potential and superoxide production

To assess the mitochondrial membrane potential ($\Delta\Psi$m), we used the JC-1 (5,5′,6,6′-tetrachloro-1,1′,3,3′-tetraethylbenzimidazolylcarbocyanine iodide) probe (Thermo Fisher Scientific, T3168). One to three morphologically healthy oocytes per genotype per experimental replicate were incubated in 5 μM JC-1 for 15 min at 37°C and 5% CO_2 under mineral oil, then washed through three consecutive droplets of FHM, prior to imaging on a glass-bottomed petri dish in 50-μL droplets of FHM under mineral oil. Positive control oocytes were incubated in 1 μM carbonyl cyanide 3-chlorophenylhydrazon (CCCP) (Millipore Sigma, C2759) under mineral oil for 15 min at 37°C at 5% CO_2 prior to incubation with JC-1. CCCP is a known mitochondrial uncoupler, which breaks down the $\Delta\Psi$m by transporting protons across the inner mitochondrial membrane [41]. JC-1 is a cationic carbocyanine dye that accumulates in the mitochondria. In low concentrations, the dye stays in its j-monomer form and will fluoresce green; however, in high concentrations the dye will form j-aggregates that fluoresce red. Due to its cationic nature, the concentration of JC-1 per organelle is dependent on the $\Delta\Psi$m; thus, lower $\Delta\Psi$m will fluoresce green and high $\Delta\Psi$m, red. Total $\Delta\Psi$m per oocyte is reported as the total sum fluorescence ratio of red:green.

MitoSOX (Thermo Fisher Scientific, M36008) was used to assess specifically mitochondrial superoxide production in live oocytes. One to three morphologically healthy oocytes per genotype per experimental replicate were incubated in 5 μM MitoSOX for 30 min at 37°C and 5% CO_2 under mineral oil, then washed through three droplets of FHM prior to imaging on a glass-bottomed petri dish in 50-μL droplets of FHM under mineral oil. Positive control oocytes were incubated with 1 μM CCCP for 15 min at 37°C and 5% CO_2 prior to MitoSOX incubation. MitoSOX is fluorogenic dye targeted to the mitochondria. Once in the mitochondria, it will be immediately oxidized by superoxide if present, emitting red fluorescence. Mitochondrial superoxide production was estimated by total red fluorescence per oocyte divided by the mean red fluorescence of *Gclm*$^{-/-}$ oocytes analyzed on the same day.

Measurement of mitochondria and lipid droplet colocalization

One to three morphologically healthy oocytes per genotype per experimental replicate were incubated in 300 nM MitoTracker Deep Red (Thermo Fisher Scientific, M22426) at 37°C and 5% CO_2 for 30 min under mineral oil, then washed through three droplets of FHM, and fixed in 4% paraformaldehyde at room temperature for 1 h in darkness. Following fixation, oocytes were washed through three small droplets of 1× PBS with 3 mg/mL PVP then incubated in 3.82 μM BODIPY 493/503 under mineral oil for 1 h at room temperature in darkness. Following that incubation, oocytes were washed through three small droplets of 1× PBS with 3 mg/mL PVP. Oocytes were immediately imaged using confocal microscopy; mitochondria were visualized using 644/665 (ex/em), and LDs were visualized using 493/503 (ex/em).

Confocal imaging and image analysis

Unless otherwise stated, *z*-stack imaging was performed on a Zeiss two-photon laser scanning microscope 780 (ZEISS Research Microscopy Solutions), and all imaging analysis was performed using the Imaris imaging software (Oxford Instruments) or FIJI ImageJ (NIH). Analysis of $\Delta\Psi$m, mitochondria, and LDs were performed in Imaris by using a three-dimensional (3D) rendering of the *z*-stack images. The raw fluorescence for each channel was used to render volumes specific to the fluorescence wavelength. Volumes in Imaris are 3D models computed from 3D images. The mean fluorescence of each individual volume was calculated and the sum fluorescence for the whole oocyte was calculated. Mitochondrial clustering was assessed in Imaris using volumes created in the 3D-rendered oocyte from *z*-stack. Clusters were defined as overlapping mitochondrial surfaces having a combined volume of greater than 10 μm^3. Any mitochondrial surface, individual or clustered, located within 8 μm of the plasma membrane was defined as subcortical.

Mitosox fluorescence was analyzed in ImageJ FIJI by compressing the *z*-stack into a *z*-stack maximum intensity projection, subtracting background fluorescence, then measuring the fluorescence in a region of interest encompassing the oocyte.

qPCR for telomere length

Mice were superovulated, and oocytes were collected and washed through drops of FHM as described above. Oocytes

were then transferred to 1× PBS with 3 mg/mL PVP and frozen at −80°C. On the day of DNA extraction, oocytes were thawed and pooled, with 20 oocytes of good morphology (clear, granular cytoplasm; small perivitelline space; first polar body; colorless zona pellucida; and not fragmented) of the same genotype per pool and with each pool containing oocytes from 1 to 3 mice. Genomic DNA was extracted from oocytes following the QIAmp DNA Micro Handbook according to the Isolation of Genomic DNA from Tissues protocol with a few modifications. Briefly, oocytes were suspended in 180 μL of Buffer ATL and equilibrated to room temperature, then proteinase K was added to each sample and incubated overnight at 56°C. Then, 200 μL of Buffer AL was added to all samples followed by 200 μL of 95% EtOH, mixed and incubated for 5 min at room temperature. Samples were briefly centrifuged, and lysates were eluted using the QIAamp MinElute column. Columns were washed with 80% EtOH following standard column wash steps, then centrifuged at full speed for 3 min to dry the membrane. Following centrifugation, ultrapure water was warmed to 65°C, then applied to the column and allowed to incubate for 10 min. Eluted genomic DNA was quantified using NanoDrop. Relative average length of telomeres was assessed by qPCR according to previously described methods [42]. This method quantifies telomeric DNA using forward and reverse primers 5′ CGG TTT GTT TGG GTT TGG GTT TGG GTT TGG GTT TGG GTT 3′ and 5′ GGC TTG CCT TAC CCT TAC CCT TAC CCT TAC CCT TAC CCT 3′, respectively. That amount is then divided by the quantity of a single copy gene, the ribosomal protein, large, P0 (RPLP0, also known as 36B4) gene (Forward and reverse primers were 5′ ACT GGT CTA GGA CCC GAG AAG 3′ and 5′ TCA ATG GTG CCT CTG GAG ATT 3′, respectively) providing an average telomere length ratio. Reactions were run in triplicate with a total of 25 μL with 12.5 μL of Sybr Green PCR Master Mix, 300 nM forward primer, 500 nM reverse primer, 20 ng of genomic DNA, and ultrapure water. A standard curve was generated using a 2× dilution series of gDNA from 0.156 to 0.00061 ng/μL. PCR amplification of telomeres was performed on a BioRad CFX Connect thermal cycler using the following program: (1) initial incubation at 95°C for 10 min; (2) each cycle (total of 40 cycles) at 95°C for 15 s, followed by incubation at an average annealing temperature of forward and reverse primers at 61°C for 1 min; and (3) final elongation step at 55°C for 5 s. Relative telomere length was calculated using the Pfaffl method [43].

Serum lipidomics

Lipidomics were carried out on serum from superovulated *Gclm*$^{+/+}$, *Gclm*$^{+/-}$, and *Gclm*$^{-/-}$ mice, as well as unsuperovulated *Gclm*$^{+/-}$ females, by the NIH West Coast Metabolomics Center at the University of California, Davis using the following protocol. Blood serum was extracted following the protocols first published in Matyash et al. [44]. Data were acquired using the following chromatographic parameters. Waters Acquity UPLC CSH C18 column (100 mm length × 2.1 mm internal diameter; 1.7 μm particles) was heated to 65°C and protected by a guard column. Mobile phase flow-rate was 0.6 mL/min, and samples were injected at a volume of 1.67 μL for ESI(+) and 5 μL for ESI(−) at injection temperature of 4°C. Mobile phases for positive mode were as follows: mobile phase A, 60:40 v/v acetonitrile:water +10 mM ammonium formate +0.1% formic acid and mobile phase B, 90:10 v/v isopropanol:acetonitrile +10 mM ammonium formate +0.1% formic acid. Mobile phases for negative mode were as follows: mobile phase A, 60:40 v/v acetonitrile:water +10 mM ammonium acetate and mobile phase B, 90:10 v/v isopropanol:acetonitrile +10 mM ammonium acetate. The gradient was the same for both positive and negative modes as follows: 0 min 15% (B), 0–2 min 30% (B), 2–2.5 min 48% (B), 2.5–11 min 82% (B), 11–11.5 min 99% (B), 11.5–12 min 99% (B), 12–12.1 min 15% (B), 12.1–15 min 15% (B). ESI capillary voltage was ESI(+): +3.5 kV and ESI(−): −3.5 kV. Precursor/product isolation width was set for 4 Da. Collision energy was set at 25 eV for ESI(+) and 25 eV for ESI(−). The scan range for positive mode was *m/z* 120–1200 Da and scan range for negative mode was *m/z* 60–1200 Da. Spectral acquisition speed: 2 spectra/s. Mass resolution was set at 10 000 for ESI(+) on an Agilent 6530 QTOF MS; 20 000 for ESI(−) on an Agilent 6550 QTOF MS.

Lipidomics peak intensity data were analyzed using MetaboAnalyst 5.0 (NIH and GenomeCanada; [45]). No data were filtered, and all values were normalized to the mean of *Gclm*$^{-/-}$ serum; the data were found to be skewed, so a log10 transformation was used along with Pareto scaling. Univariate analyses utilized ANOVA with Fisher's least significant difference tests for intergroup comparisons. Multivariate principal component analysis (PCA) was performed. Hierarchical clustering analysis using a Euclidean distance measure and ward clustering algorithm was performed on the lipid species that were found to have an ANOVA FDR adjusted *P*-value of less than 0.02. Random Forest supervised classification and feature selection was also performed. Random Forest is a supervised learning algorithm that uses a group of classification trees. A bootstrap subset of the whole data set from which random features were selected at each branch was used to grow the group. Class prediction was based on the majority vote of the group. During tree construction, about one-third of the samples were left out of the bootstrap set. This out of bag (OOB) data was then used as a test sample to obtain an unbiased estimate of the classification error (OOB error). Variable importance was evaluated by measuring the increase of the OOB error when it was permuted.

Statistical analyses

Data are displayed as means ± SEM unless otherwise noted. The reported *N*s in this study are representative of the number of animals per genotype for each endpoint. The effect of *Gclm* genotype on the average oocyte DCF fluorescence levels for multiple oocytes from the same mouse was analyzed by *t*-test. The effects of *Gclm* genotype on all other oocyte endpoints were analyzed using the generalized estimating equation (GEE) form of the general linear model to account for repeated measures within animals (the same endpoint was measured in multiple oocytes from the same mouse). GEE models utilized exchangeable correlation matrices. IBM SPSS Statistics 25 for Macintosh was used for statistical analyses.

Results

Gclm$^{-/-}$ oocytes have increased ROS levels, likely attributed to increased mitochondrial superoxide

We observed no differences in the numbers of morphologically healthy oocytes ovulated across genotypes (Figure 1A).

On average, *Gclm*$^{+/+}$ ovulated 19 ± 3 ($N = 13$), *Gclm*$^{+/-}$ ovulated 15 ± 2 ($N = 21$), *Gclm*$^{-/-}$ ovulated 17 ± 2 ($N = 31$). ROS levels were measured in superovulated oocytes of *Gclm*$^{-/-}$ and *Gclm*$^{+/+}$ mice using H_2DCF-DA. Relative ROS was measured as fluorescence intensity in experimental oocytes compared with fluorescence intensity in 0.003% hydrogen peroxide-treated positive control oocytes of the same genotype on the same day. Relative ROS concentrations in *Gclm*$^{-/-}$ oocytes were significantly higher than in the *Gclm*$^{+/+}$ counterparts ($P = 0.008$, *t*-test) (Figure 1B). Mitochondria are the primary source of ROS in oocytes even though the mitochondria of oocytes are relatively quiescent [20, 26, 46]. H_2DCF-DA fluorescence assays are nonspecific, reacting with any reactive oxygen species to fluoresce green. Therefore, we measured mitochondrial superoxide using the fluorescent probe MitoSOX to determine the average fold red fluorescence of *Gclm*$^{+/+}$, *Gclm*$^{+/-}$, and *Gclm*$^{-/-}$ oocytes. We observed that *Gclm*$^{-/-}$ oocytes have increased mitochondrial superoxide compared with both *Gclm*$^{+/+}$ and *Gclm*$^{+/-}$ oocytes ($P = 0.045$, GEE) suggesting that the lack of GSH in the mitochondria of the *Gclm*$^{-/-}$ oocytes is the primary cause for increased oxidative stress and that GSH is the primary antioxidant that maintains this balance in oocyte mitochondria (Figure 1C).

No difference in telomere length between *Gclm*$^{-/-}$ and *Gclm*$^{+/+}$ oocytes

Telomeres are tandem repeats of TTAGGG at the end of chromosomes. They are thought to prevent chromosome ends from being recognized as DNA double strand breaks. However, due to their high guanine content, telomeres are especially susceptible to oxidative damage [47, 48]. Previously we have shown that *Gclm*$^{-/-}$ mice undergo accelerated age-related decreases in ovarian follicle numbers [13]. Shortened telomere length is considered to be a hallmark of aging [49]. To assess if increased ROS in *Gclm*$^{-/-}$ oocytes lead to decreased telomere length and therefore advanced aging in the *Gclm*$^{-/-}$ oocyte, telomere length was compared in oocyte DNA from *Gclm*$^{-/-}$ and *Gclm*$^{+/+}$ mice. The relative telomere lengths did not differ significantly between the two genotypes for oocytes with normal morphology (Figure 1D). These data suggest that increased ROS in the oocyte does not cause a statistically significant difference in oocyte telomere length in peripubertal mice.

Gclm$^{-/-}$ oocytes have decreased mitochondrial membrane potential and decreased subcortical mitochondrial clustering

We observed an increase in superoxide production in *Gclm*$^{-/-}$ oocytes (Figure 1B). Mitochondrial superoxide is produced during the reduction of oxygen in the electron transport chain [50, 51]. Typically, the increase in SO production implicates mitochondrial respiratory dysfunction [50, 51]. Electrons are carried along the electron transport chain and used to pump protons into the intermembrane space of the mitochondrion, generating an electrochemical gradient. This gradient is referred to as mitochondrial membrane potential ($\Delta\Psi m$) and is an important indicator of mitochondrial activity. We assessed $\Delta\Psi m$ of *Gclm*$^{+/+}$, *Gclm*$^{+/-}$, and *Gclm*$^{-/-}$ oocytes and observed that *Gclm*$^{-/-}$ and *Gclm*$^{+/-}$ oocytes had significantly lower $\Delta\Psi m$ than *Gclm*$^{+/+}$ counterparts ($P = 0.032$, effect of genotype, GEE) (Figure 2A and B). Next, we explored differences in mitochondrial clustering among genotypes and found that although there was no difference in mitochondrial clustering in the whole oocyte, *Gclm*$^{-/-}$ oocytes had significantly less mitochondrial clusters in the more oxygenated subcortical region of the oocyte than *Gclm*$^{+/-}$ and *Gclm*$^{+/+}$ oocytes (Figure 2D and E). Together these data demonstrate a potential compensatory mechanism exhibited by *Gclm*$^{-/-}$ oocyte mitochondria to accommodate higher levels of oxidative stress.

No difference in oocyte lipid peroxidation across genotypes

ROS are highly reactive and stochastically react with and oxidize the first macromolecules (lipids, DNA, proteins) with which they come in contact; in the case of free fatty acids and other lipids this can create lipotoxic conditions that degrade the health of the cell further [52]. Under homeostatic conditions, oxidized lipids and other macromolecules would be reduced by GSH, with the help of glutathione peroxidase [26]. To characterize how GSH deficiency impacts the oxidation state of this crucial energy source in mature oocytes, we utilized the fluorophore BODIPY 581/591 C11. We measured the fold difference of oxidized (green) to unoxidized (red) fluorescence ratio compared with *Gclm*$^{-/-}$ oocytes and observed no statistical difference among all genotypes in lipid peroxidation levels (Figure 2C). Even though there is a significant increase in ROS, specifically superoxide (Figure 1A and B), there is no effect on lipid peroxidation levels in *Gclm*$^{-/-}$ oocytes. Given that ROS reactivity with cellular macromolecules is stochastic in nature, this suggests that *Gclm*$^{-/-}$ oocytes have fewer lipids overall therefore reducing the probability that a ROS molecule will react with a lipid before a protein or other macromolecules.

Gclm$^{-/-}$ mice have altered serum lipid profiles compared with *Gclm*$^{+/-}$ and *Gclm*$^{+/+}$

It is understood that follicular fluid is sourced from the serum and provides essential metabolites to growing follicles [18, 31]. We have previously demonstrated that *Gclm*$^{-/-}$ mice have decreased adipogenesis and are therefore protected from increased risk of hepatic steatosis following in utero exposure to benzo(a)pyrene [6]. As we observed no difference in the lipid peroxidation of ovulated oocytes among genotypes, we explored if there was a *Gclm* genotype-associated difference in serum lipids using high performance liquid chromatography-mass spectrometry.

We observed distinct differences among genotypes, with superovulated *Gclm*$^{-/-}$ females possessing a distinct serum lipid population from superovulated *Gclm*$^{+/+}$ and *Gclm*$^{+/-}$ females by hierarchical cluster analysis, PCA, and Random Forest analyses (Figure 3A–C, Table 1). Serum from superovulated *Gclm*$^{+/+}$ and *Gclm*$^{+/-}$ mice was enriched in mono- and poly-unsaturated fatty acids (linolenic, eicosenoic, eicosatrienoic, and FA 22:4) and triacylglycerols compared with *Gclm*$^{-/-}$ serum (Figures 3A, 4A and B; Supplemental Table S1). Further, serum from superovulated *Gclm*$^{-/-}$ mice was observed to be enriched in sphingomyelins and had increased levels of cholesterol compared with the other genotypes (Figures 3A, 4D; Supplemental Table S1). Interestingly, serum from unsuperovulated *Gclm*$^{+/-}$ females had a distinct lipid profile from superovulated females of all genotypes (Figures 3A–C, 4C). This group was found to be

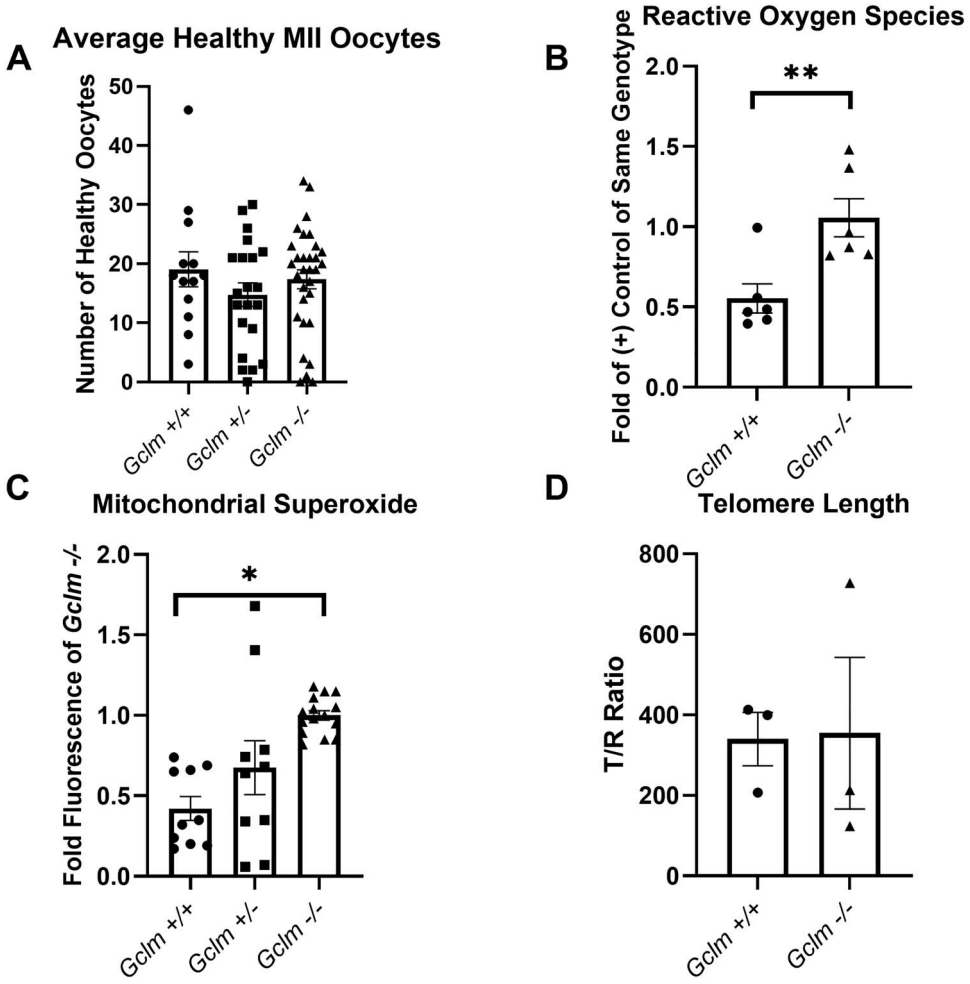

Figure 1. *Gclm*$^{-/-}$ oocytes have increased levels of ROS compared to *Gclm*$^{+/+}$ oocytes. (A) There is no difference in the number of morphologically healthy oocytes ovulated per female of each genotype ($N = 13 = 31$ females/genotype). (B) Green DCF fluorescence of experimental oocytes relative to mean fluorescence of 0.003% hydrogen peroxide-treated, positive control oocytes of same genotype on the same experimental day is elevated in *Gclm*$^{-/-}$ oocytes (** $P = 0.008$, *t*-test, $N = 6$ females/genotype; superimposed filled circles, squares and triangles show values for individual oocytes in this and subsequent figures). (C) *Gclm*$^{-/-}$ oocytes have increased levels of mitochondrial superoxide, as estimated by fold *Gclm*$^{-/-}$ fluorescence of oocytes analyzed on the same day (* $P = 0.045$, GEE, $N = 5$–8 females/genotype). (D) There is no statistically significant difference in telomere length between genotypes ($N = 3$ pools of 20 oocytes each from 1–3 females/genotype).

enriched in phospholipids and sphingomyelins, and deficient in triacylglycerols as well as ceramides (Figures 3A, 4B–D; Supplemental Table S1). Together these data show that *Gclm*$^{-/-}$ serum carries decreased levels of the lipids that are ultimately required for oocyte competence.

Gclm$^{+/-}$ and *Gclm*$^{-/-}$ oocytes have fewer lipid droplets

It is well established that LDs are important for oocyte developmental competence, playing several crucial roles in maintenance of the oocyte and preimplantation embryonic development [17, 18, 31, 37, 38, 53]. Above we found that the serum lipid profile in *Gclm*$^{-/-}$ mice was distinctly different from the serum lipid profiles of the other two genotypes (Figure 3A–C). Therefore, we assessed the lipid stores in ovulated oocytes in all three genotypes.

We found both *Gclm*$^{+/-}$ and *Gclm*$^{-/-}$ oocytes have significantly lower LD content than *Gclm*$^{+/+}$ oocytes ($P = 0.001$, effect of genotype, GEE) (Figure 5A and D). The average volume of a single LD was significantly lower in *Gclm*$^{-/-}$ oocytes compared to *Gclm*$^{+/-}$ and *Gclm*$^{+/+}$ oocytes ($P < 0.001$, effect of genotype, GEE) (Figure 5C). However, there was no significant difference in the proportion of mitochondria colocalized with LDs amongst genotypes (Figure 5B). Together these data show that the decreased levels of triacyglycerols and free fatty acids in *Gclm*$^{-/-}$ serum are correlated with decreased LD content and smaller LDs, but the ability for those oocytes to metabolize fatty acids is likely equivalent amongst genotypes.

Discussion

In this study we explored possible underlying changes in oocyte quality, which may explain why embryos derived from *Gclm*$^{-/-}$ oocytes, possessing <20% of the average *Gclm*$^{+/+}$ oocyte GSH concentration, have increased preimplantation mortality compared with *Gclm*$^{+/+}$ oocytes [5]. We observed that *Gclm*$^{-/-}$ oocytes have increased cellular ROS and mitochondrial superoxide in comparison to their wildtype counterparts. Consistent with this, we found that *Gclm*$^{-/-}$ and *Gclm*$^{+/-}$ oocytes had decreased $\Delta\Psi$m and decrease subcortical mitochondrial clustering in comparison to *Gclm*$^{+/+}$ oocytes. This increase in ROS and decreased $\Delta\Psi$m did not,

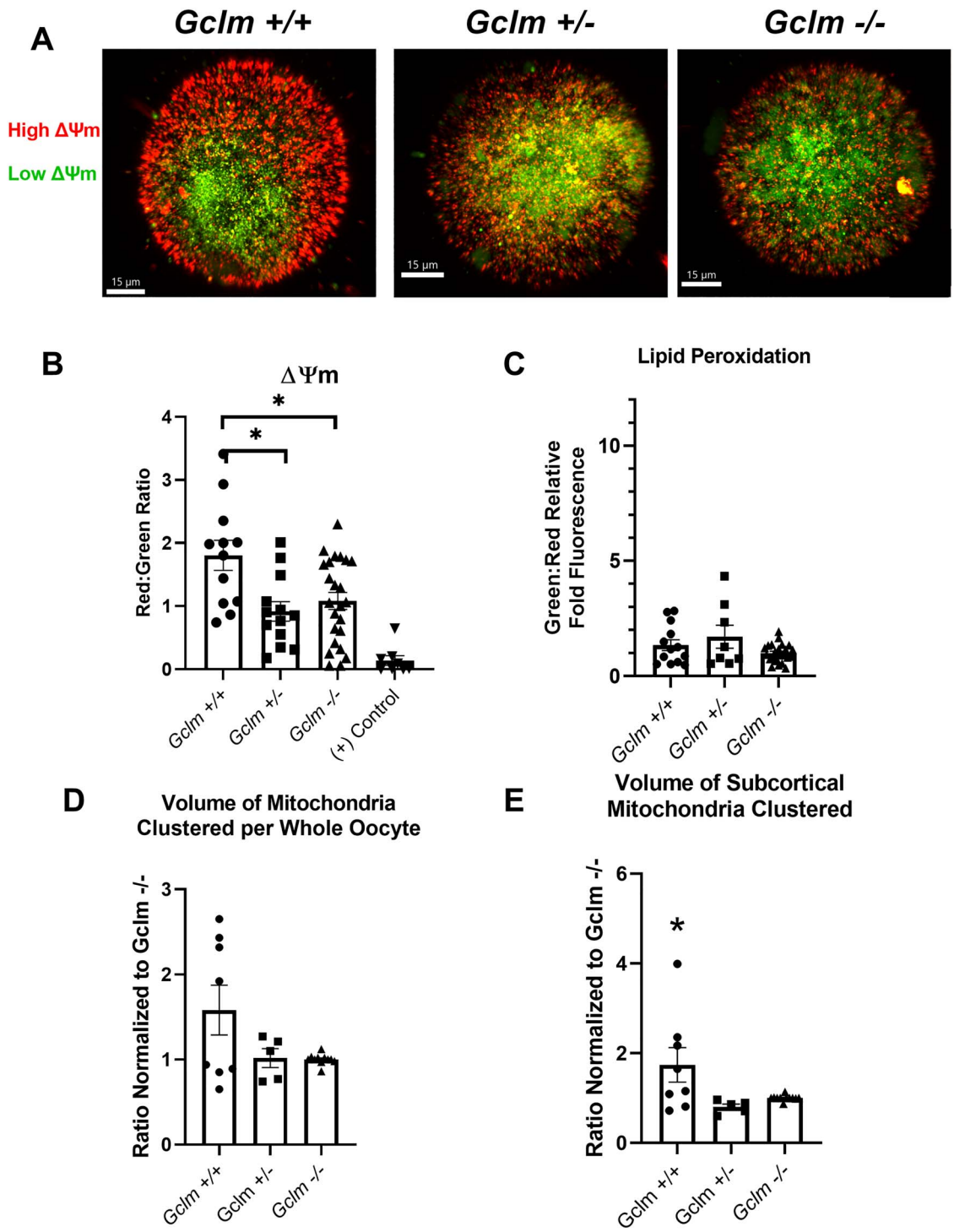

Figure 2. *Gclm*$^{-/-}$ oocytes have decreased ΔΨm but no difference in lipid peroxidation compared with *Gclm*$^{+/+}$ oocytes. (A) Representative confocal images of JC-1 ΔΨm measurement (red = high ΔΨm, green = low ΔΨm). (B) *Gclm*$^{-/-}$ and *Gclm*$^{+/-}$ oocytes have lower mitochondrial membrane potential measured as total mean red:green fluorescence ratio using JC-1 (*$P < 0.05$, GEE, $N = 5$–11 females/genotype). The mitochondrial uncoupler CCCP was used as a positive control. (C) There is no *Gclm* genotype-related difference in lipid oxidation measured as total mean green:red fluorescence ratio using BODIPY 581/591 C11, excitation at 581 nm and emission at 591 nm (red), which will shift to 510 nm (green) when oxidized ($N = 4$–9 females/genotype). (D) Total volume of mitochondrial clusters per whole oocyte normalized to volume in *Gclm*$^{-/-}$ oocytes imaged on same day does not differ by *Gclm* genotype ($N = 3$–7 females/genotype). (E) Ratio of mitochondrial volume clustered in the subcortical region of the oocyte to total mitochondrial volume is significantly decreased in *Gclm*$^{-/-}$ and *Gclm*$^{+/-}$ compared to *Gclm*$^{+/+}$ oocytes ($N = 3$–7 females/genotype, *$P < 0.05$, GEE). Superimposed filled symbols show values for individual oocytes in all graphs in this figure.

Table 1. Random Forest classification performance

	Gclm$^{-/-}$	*Gclm*$^{+/-}$	*Gclm*$^{+/+}$	unsuper-ovulated	classification error
Gclm$^{-/-}$	9.00	0.00	0.00	0.00	0.00
Gclm$^{+/-}$	2.00	1.00	1.00	1.00	0.80
Gclm$^{+/+}$	0.00	4.00	0.00	0.00	1.00
unsuper-ovulated	0.00	0.00	0.00	4.00	0.00

*The first four columns show the number of mice of each genotype/experimental group indicated in the row headings that were classified by the Random Forest method as the genotype/experimental group indicated in the column headings. The last column shows the fraction of mice in each row that were classified incorrectly.

however, result in an increase in oocyte lipid peroxidation; we surmise this is likely because *Gclm*$^{-/-}$ oocytes possess significantly less LD content than *Gclm*$^{+/+}$ oocytes. Lipids stored in LDs are derived, in part, from serum. When we assessed the serum lipid profiles for the three genotypes, we found *Gclm*$^{-/-}$ serum to be deficient in triacylglycerols and fatty acids compared with *Gclm*$^{+/-}$ and *Gclm*$^{+/+}$ serum.

The oxidative state of the oocyte, and therefore its developmental competence, is very sensitive to any perturbations [21, 54]. GSH plays a crucial role in maintaining the redox state of the ovary [26] and oocyte [5, 13]. Mice deficient in GSH undergo accelerated age-related ovarian failure [13], and the embryos derived from oocytes of GSH-deficient mice have a higher incidence of preimplantation mortality [5]. Therefore it could be surmised that *Gclm*$^{-/-}$ oocytes, with GSH concentrations <20% those of *Gclm*$^{+/+}$ oocytes [5], would have a drastic shift in their cellular redox state to be more oxidized [26] and possibly show signs of accelerated aging. In this study we observed an increase in ROS in *Gclm*$^{-/-}$ oocytes (Figure 1B), most likely driven by an increase in mitochondrial superoxide (Figure 1B). However, we did not observe telomere shortening in the *Gclm*$^{-/-}$ oocytes compared with *Gclm*$^{+/+}$ (Figure 1C). It is likely that the mice used in this experiment were too young to begin to see an effect of oxidative stress on oocyte telomere length. The mice used in this study were between PND 35–45. In contrast, the youngest age at which we previously observed significantly lower ovarian follicle numbers in *Gclm*$^{-/-}$ mice compared to *Gclm*$^{+/+}$ mice was 2 months of age, and the difference became more pronounced with increasing age thereafter [13]. Given the highly oxidized state of the *Gclm*$^{-/-}$ oocytes, it is possible that we would observe shortening of telomeres in older mice, and later studies should explore this. This more highly oxidized state could lead to shifts in the delicately balanced mitochondrial functions within the oocytes [26, 55, 56].

Oocyte mitochondria are small and round, possessing relatively few cristae, and an electron-dense matrix, as opposed to rod-like somatic cell mitochondria, which contain many cristae and a less electron-dense matrix [8, 17, 18]. However, even though they are relatively quiescent, the mitochondria are the primary source of ATP for the mature, ovulated oocyte [18, 21, 22]. After fertilization until the compacted morula stage, the mammalian embryo is entirely dependent on the mitochondria contributed from the ovulated oocyte, roughly 100 000 mitochondria per murine oocyte. The early embryo relies primarily on pyruvate oxidation and fatty acid β-oxidation to survive until the compacted morula commences glycolysis [17, 22]. We observed that *Gclm*$^{-/-}$ oocytes have decreased $\Delta\Psi$m compared with *Gclm*$^{+/-}$ and *Gclm*$^{+/+}$ oocytes (Figure 2A). From this we can conclude that mitochondria in *Gclm*$^{-/-}$ oocytes, undergoing higher levels of oxidative stress, have downregulated activity of oxidative phosphorylation to avoid further production of ROS and propagation of a vicious cycle [48, 54]. These observations are supported by *Gclm*$^{-/-}$ oocytes having less mitochondria clusters in the subcortical region of the oocyte compared to *Gclm*$^{+/+}$ (Figure 2D). Although oocyte mitochondria are generally fragmented and smaller [57], they still have been documented to aggregate [58]. Sturmey et al. observed that in pig oocytes, peripheral or subcortical mitochondrial clustering was correlated with higher oxygen availability [33]. Redox homeostasis and structural mitochondrial dynamics have been exhaustively studied in somatic cells and have reproducibly shown that exposure to increased ROS triggers $\Delta\Psi$m depolarization alongside mitochondrial fragmentation [59], while clustered or fused mitochondria consume oxygen for ATP production [60]. Together these data demonstrate that increased oxidative stress in the setting of low GSH, depolarizes oocyte mitochondria. But our data also suggest a compensatory mechanism whereby *Gclm*$^{-/-}$ oocytes cluster mitochondria away from the subcortical region to maintain similar levels of metabolism while avoiding the potential for even more production of ROS.

Gclm$^{-/-}$ mice also have decreased lipid biosynthesis and decreased weight gain on a high-fat diet [61]. We have observed that *Gclm*$^{-/-}$ female mice have about 50% lower visceral adipose tissue weights than *Gclm*$^{+/+}$ littermates [6]. We hypothesized that the previously observed decreased lipid biosynthesis in *Gclm*$^{-/-}$ mice would have implications for mature oocyte health, given the important role LDs play in embryo development. To this end, we used LC–MS to assess serum lipidomics across all three genotypes. We observed different serum lipid populations among the genotypes, with *Gclm*$^{-/-}$ being the most distinct from *Gclm*$^{+/+}$ and *Gclm*$^{+/-}$ assessed by hierarchical clustering analysis, PCA, and Random Forest analysis (Figure 3A–C; Table 1). Specifically, we observed a decrease in serum triacylglycerols in *Gclm*$^{-/-}$ serum (Figure 4A and B, Supplemental Table S1). Serum metabolites and macromolecules populate the follicular fluid in the ovary, and optimal composition of the follicular fluid is required for normal cumulus cell and oocyte function [14, 62]. Triacylglycerols are the primary components of the neutral lipid core of LDs in all cell types [63, 64]. Whether these are primarily sourced from the follicular fluid or synthesized intracellularly has not been fully explored, but it is likely a combination of sources. Having observed decreased serum triacylglycerol content in *Gclm*$^{-/-}$ females, we hypothesized that *Gclm*$^{-/-}$ oocytes have less LD content than the other genotypes.

Lipid composition of ovarian follicular fluid differs significantly between older and young ovaries, with older patients

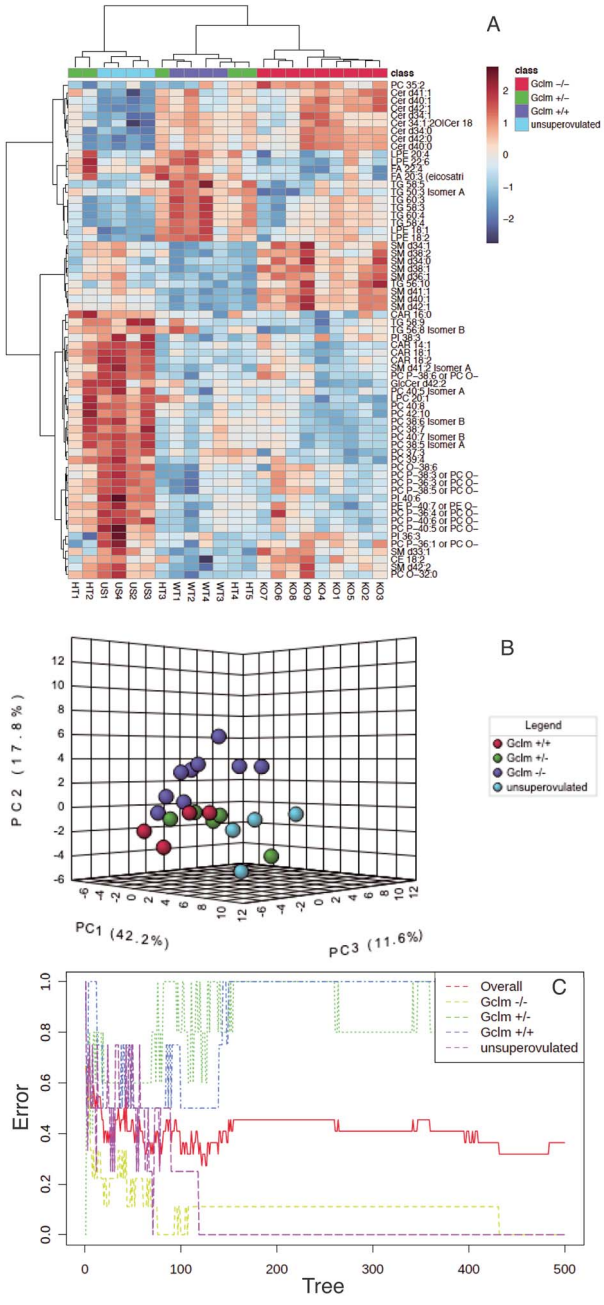

Figure 3. Serum lipidomics demonstrate altered lipid profile in superovulated *Gclm*$^{-/-}$ mice compared to superovulated *Gclm*$^{+/-}$ and *Gclm*$^{+/+}$ mice and unsuperovulated *Gclm*$^{+/-}$ mice. (A) Hierarchical cluster analysis of serum lipid concentrations shows distinct clusters of *Gclm*$^{-/-}$ and unsuperovulated *Gclm*$^{+/-}$. (B) Principal component analysis similarly shows that *Gclm*$^{-/-}$ females have distinct serum lipid profile compared with other genotypes. (C) Random Forest classification shows the cumulative classification error rates for each experimental group, as well as the overall error rate, as the group of classification trees is grown by random feature selection from a bootstrap sample. The analysis shows that *Gclm*$^{-/-}$ and unsuperovulated mice have distinct serum lipid profiles, which allow them to be reliably separated with zero error rates from the other experimental groups, while *Gclm*$^{+/-}$ and *Gclm*$^{+/+}$ mice do not. ($N = 4$–9 females/group).

possessing less arachidonate and certain lysophosphatidylcholines [29], which all play a part in follicular development and oocyte competence. The most interesting differences we observed in serum were decreased concentrations of polyunsaturated fatty acids in *Gclm*$^{-/-}$ serum (Figures 3, 4A; Supplemental Table S1). Li et al., recently characterized the metabolic patterns of mouse oocytes during meiotic maturation and demonstrated that polyunsaturated fatty acids decline sharply in the oocyte from germinal vesicle to MII stage [65]. Their data further suggest that polyunsaturated fatty acid signaling plays an inhibitory role in oocyte maturation, and that it must be downregulated for oocyte maturation to proceed [65]. Polyunsaturated fatty acids have been previously suggested to improve oocyte quality of various mammalian species; most commonly their benefit has been attributed to the production of prostaglandins [66–69]. However, other studies have shown that periconception diet supplementation with long chain $n-3$ polyunsaturated fatty acids resulted in altered mitochondrial distribution and increased ROS in the oocyte along with a reduction in normal embryo development [70]. Therefore, it is likely that oocyte competence is dependent on a balance of polyunsaturated fatty acids.

LDs are a source of ATP for oocyte mitochondria post ovulation and during preimplantation development [18, 21, 30, 38]. They also supply important signaling molecules [27, 31], contribute to generation of plasma membranes for the growing embryo [28, 31], and play an important role in regulation of cellular stress by lending lipoic acid as a cofactor for mitochondrial dehydrogenases, thus increasing NADH levels for maintenance of redox balance [32]. We observed that *Gclm*$^{-/-}$ oocytes possessed significantly fewer and smaller LDs than *Gclm*$^{+/+}$ counterparts (Figure 5A and C). These data are supported by Mok et al., who compared lipidome changes in MII oocytes from 4-week and 42 to 50-week-old mice and H_2O_2-treated oocytes from 4-week-old mice [72]. H_2O_2-treated and aged oocytes were observed to have decreased LD content compared with young oocytes [71], similar to the decreased LD content we observed in *Gclm*$^{-/-}$ oocytes (Figure 5A).

To characterize if the absence of a preferential energy resource contributed to decreased $\Delta\Psi m$ in *Gclm*$^{-/-}$ oocytes we analyzed mitochondria:LD colocalization to calculate the percentage of peridroplet mitochondria and found there to be no difference in colocalization of mitochondria and LDs among genotypes (Figure 5B). Interestingly, the average volume of a single LD was smaller in *Gclm*$^{-/-}$ oocytes (Figure 5C). This is possibly driven, in part, by the *Gclm*$^{-/-}$ serum having decreased levels of triacylglycerols (Figure 3, Supplemental Table S1). Depending on the cell type, mitochondria colocalized with LDs can either be predominantly active in building LDs (lipogenesis), or utilizing LDs for ATP (fatty acid β-oxidation) [72]. Though there is only a little evidence to support this, it is currently accepted by the field that, in oocytes, mitochondria colocalized with LDs are primarily active in ATP production using fatty acid β-oxidation [17]. However, recent findings in hepatocytes show that peridroplet mitochondria, colocalized with LDs, actually produce and consume ATP through pyruvate oxidation to build LDs [73]. Given that MII ovulated oocytes preferentially oxidize pyruvate or fatty acids to yield ATP, further characterization of the bioenergetics of distinct

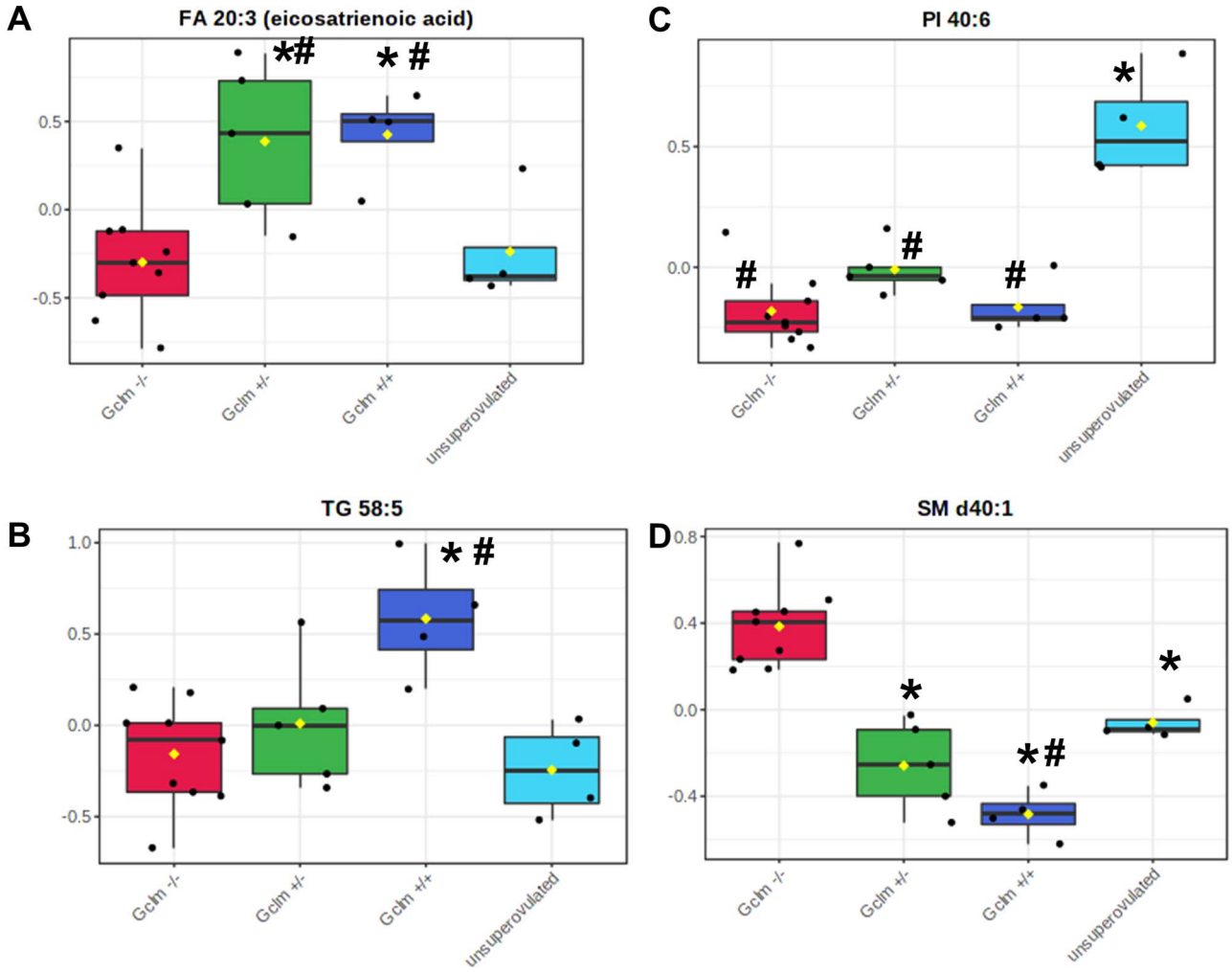

Figure 4. Representative differences in serum fatty acids, triacylglycerols, phospholipids, and sphingomyelins among *Gclm* genoytypes. (A–D) Representative box-and-whisker plots from serum lipidomics analysis described in Figure 3 showing significantly different concentrations of representative (A) fatty acid (FDR *P*-value = 0.015), (B) triacylglycerol (FDR *P*-value = 0.004), (C) phospholipid (FDR *P*-value = 0.0001), and (D) sphingomyelin (FDR *P*-value = 7.43E−05) among experimental groups. ∗Significantly different ($P < 0.05$) from $Gclm^{-/-}$ by Fisher's LSD test; # significantly different ($P < 0.05$) from unsuperovulated by Fisher's LSD test. ($N = 4$–9 females/group).

peridroplet mitochondria in oocytes should be explored with more sensitive tools.

Recent findings have further expanded on the necessary role that LDs play in oocyte competence. MII oocytes were shown to immediately start producing new LDs de novo following delipidation, and delipidation had no impact on early embryo development up to the 8-cell stage, attributed to de novo lipid synthesis [38]. Our previous study documented that superovulated $Gclm^{-/-}$ mice generated significantly fewer blastocysts at 3.5 days post coitum compared to $Gclm^{+/+}$, due to arrest at earlier stages [5]. Together these data suggest that decreased LD content in ovulated $Gclm^{-/-}$ oocytes could activate de novo lipogenesis pathways to support fertilization, creating an abundance of free fatty acids. Higher levels of ROS in $Gclm^{-/-}$ embryos may then compromise cellular integrity by oxidizing free fatty acids, leading to arrest and preimplantation mortality. While the current study observed no differences in MII oocyte lipid peroxidation among genotypes, we did not assess lipid peroxidation in embryos. Doing so is beyond the scope of this study and should be investigated in future studies.

This study has also demonstrated a significant distinction between the lipid populations in the serum of the experimental $Gclm^{+/-}$ mice which were superovulated and those that were not. In many ways the serum of the unsuperovulated females was more similar to the $Gclm^{-/-}$ superovulated serum, having increased concentrations of cholesterol and sphingomyelins, and decreased concentrations of triacylglycerols (Figure 3). However, the unsuperovulated serum was even more distinct, having decreased concentrations of ceramides and increased concentrations of phospholipids compared with the superovulated $Gclm^{+/-}$ serum (Figure 3, Supplemental Table S1). To our knowledge, this is the first study to characterize the serum lipidome comparing superovulated and unsuperovulated mice. These data support that PMSG and hCG acutely alter the serum lipidome and should be explored further.

In summary, we demonstrated that GSH-deficient oocytes have increased oxidative stress, but this is likely only one contributor to the previously observed increased preimplantation mortality in $Gclm^{-/-}$ females [5]. Increased ROS and mitochondrial superoxide, as well as decreased $\Delta\Psi m$

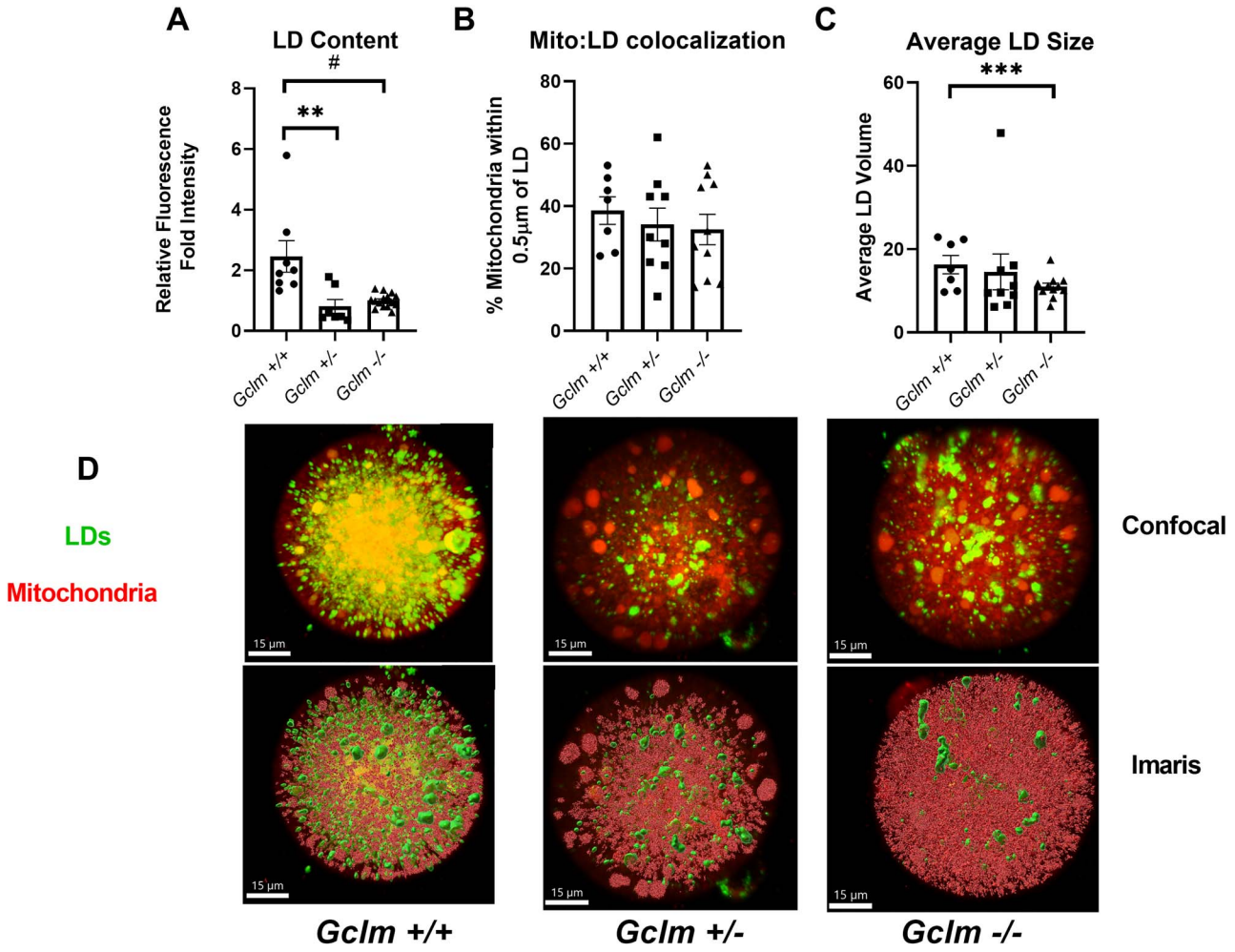

Figure 5. *Gclm*$^{-/-}$ oocytes have fewer LDs than *Gclm*$^{+/+}$ oocytes. (A) Neutral lipids were stained using BODIPY 493/503. Green fluorescence intensity, expressed as the fold mean intensity *of Gclm*$^{-/-}$ oocytes imaged on the same day, was higher in *Gclm*$^{+/+}$ and *Gclm*$^{+/-}$ compared to *Gclm*$^{-/-}$ oocytes (#*P*-value = 0.083, ** *P*-value = 0.007, by generalized estimating equation, *N* = 3–6 females/genotype). (B) There were no *Gclm*-genotype-related differences in percentage of mitochondria colocalized with LDs in oocytes measured using Mitotracker Deep Red and BODIPY 493/503 (*N* = 5–6 females/genotype). (C) Volume measurements, rendered in the Imaris imaging software using BODIPY 493/503 fluorescence, show *Gclm*$^{-/-}$ oocytes have smaller LDs on average compared with *Gclm*$^{+/+}$ (*** *P*-value<0.001, generalized estimating equation *N* = 5–6 females/genotype). (D) Representative original confocal images and same images after Imaris processing of LDs and mitochondria in oocytes of *Gclm*$^{+/+}$, *Gclm*$^{+/-}$, and *Gclm*$^{-/-}$ mice. LDs are stained using BODIPY 493/503 and mitochondria are stained using Mitotracker Deep Red. Superimposed filled symbols show values for individual oocytes in all graphs in this figure.

and subcortical mitochondrial clustering were observed in *Gclm*$^{-/-}$ oocytes compared with *Gclm*$^{+/-}$ and *Gclm*$^{+/+}$ oocytes. Additionally, we observed that *Gclm*$^{-/-}$ females possess a distinct serum lipid profile from their *Gclm*$^{+/-}$ and *Gclm*$^{+/+}$ counterparts, being less enriched in triacylglycerols and polyunsaturated fatty acids. We conclude this decrease in serum triacylglycerols and polyunsaturated fatty acids leads to our observation that *Gclm*$^{-/-}$ oocytes have severely diminished LD content, the primary source of energy, signaling molecules, phospholipids for cellular membranes, and regulator of cellular stress. However, the current study was unable to demonstrate a clear mechanistic link between differing serum lipidome and altered LD content in oocytes among genotypes. Future studies should assess LD content, mitochondrial co-localization, and oxygen consumption rate in granulosa cells and developing embryos. Lipid profiles of the follicular fluid among *Gclm*$^{-/-}$, *Gclm*$^{+/-}$, and *Gclm*$^{+/+}$ mice should also be assessed.

Supplementary material

Supplementary material is available at *BIOLRE* online.

Data availability

The data underlying this article will be shared on reasonable request to the corresponding author.

Author contributions

KFM designed and performed experiments, analyzed data, drafted manuscript. SR performed experiments, analyzed data, reviewed the manuscript. LO performed experiments, analyzed data. UL conceived of overall idea, obtained funding, analyzed data, edited the manuscript.

Acknowledgements

This research would not have been possible without the University of California, Irvine Optical Biology Core for providing training on and

access to the LSM780 confocal microscope used to image live and fixed oocytes and for the Imaris imaging software. We also acknowledge the time, effort, and expertise of the West Coast Metabolomics Center at University of California, Davis. We also thank Dr. David Keefe and Dr. Fang (Helen) Wang of New York University Langone Medical Center for assistance in adapting their oocyte telomere length assay for our study.

Conflict of interest

The authors have no conflicts of interest to declare.

References

1. Franklin CC, Backos DS, Mohar I, White CC, Forman HJ, Kavanagh TJ. Structure, function, and post-translational regulation of the catalytic and modifier subunits of glutamate cysteine ligase. *Mol Aspects Med* 2009; **30**:86–98.
2. Shi ZZ, Osei-Frimpong J, Kala G, Kala SV, Barrios RJ, Habib GM, Lukin DJ, Danney CM, Matzuk MM, Lieberman MW. Glutathione synthesis is essential for mouse development but not for cell growth in culture. *Proc Natl Acad Sci U S A* 2000; **97**: 5101–5106.
3. Dalton TP, Dieter MZ, Y Y, Shertzer HG, Nebert DW. Knockout of the mouse glutamate cysteine ligase catalytic subunit (Gclc) gene: embryonic lethal when homozygous, and proposed model for moderate glutathione deficiency when heterozygous. *Biochem Biophys Res Commun* 2000; **279**:324–329.
4. Lim J, Lawson GW, Nakamura BN, Ortiz L, Hur JA, Kavanagh TJ, Luderer U. Glutathione-deficient mice have increased sensitivity to transplacental benzo[a]pyrene-induced premature ovarian failure and ovarian tumorigenesis. *Cancer Res* 2013; **73**:908–917.
5. Nakamura BN, Fielder TJ, Hoang YD, Lim J, McConnachie LA, Kavanagh TJ, Luderer U. Lack of maternal glutamate cysteine ligase modifier subunit (Gclm) decreases oocyte glutathione concentrations and disrupts preimplantation development in mice. *Endocrinology* 2011; **152**:2806–2815.
6. Ortiz L, Nakamura B, Li X, Blumberg B, Luderer U. In utero exposure to benzo[a]pyrene increases adiposity and causes hepatic steatosis in female mice, and glutathione deficiency is protective. *Toxicol Lett* 2013; **223**:1–7.
7. McConnachie LA, Mohar I, Hudson FN, Ware CB, Ladiges WC, Fernandez C, Chatterton-Kirchmeier S, White CC, Pierce RH, Kavanagh TJ. Glutamate cysteine ligase modifier subunit deficiency and gender as determinants of acetaminophen-induced hepatotoxicity in mice. *Toxicol Sci* 2007; **99**:628–636.
8. Van Blerkom J. Mitochondrial function in the human oocyte and embryo and their role in developmental competence. *Mitochondrion* 2011; **11**:797–813.
9. Calvin HI, Grosshans K, Blake EJ. Estimation and manipulation of glutathione levels in prepuberal mouse ovaries and ova:relevance to sperm nucleus transformation in the fertilized egg. *Gamete Res* 1986; **14**:265–275.
10. Perreault SD, Barbee RR, Slott VL. Importance of glutathione in the acquisition and maintenance of sperm nuclear decondensing activity in maturing hamster oocytes. *Dev Biol* 1988; **125**: 181–186.
11. Gardiner CS, Reed DJ. Status of glutathione during oxidant-induced oxidative stress in the preimplantation mouse embryo1. *Biol Reprod* 1994; **51**:1307–1314.
12. Yoshida M, Ishigaki K, Nagai T, Chikyu M, Pursel VG. Glutathione concentration during maturation and after fertilization in pig oocytes: relevance to the ability of oocytes to form male pronucleus. *Biol Reprod* 1993; **49**:89–94.
13. Lim J, Nakamura BN, Mohar I, Kavanagh TJ, Luderer U. Glutamate cysteine ligase modifier subunit (Gclm) null mice have increased ovarian oxidative stress and accelerated age-related ovarian failure. *Endocrinology* 2015; **156**:3329–3343.
14. Dumesic DA, Meldrum DR, Katz-Jaffe MG, Krisher RL, Schoolcraft WB. Oocyte environment: follicular fluid and cumulus cells are critical for oocyte health. *Fertil Steril* 2015; **103**: 303–316.
15. Ramalho-Santos J, Varum S, Amaral S, Mota PC, Sousa AP, Amaral A. Mitochondrial functionality in reproduction: from gonads and gametes to embryos and embryonic stem cells. *Hum Reprod Update* 2009; **15**:553–572.
16. Coticchio G, Sereni E, Serrao L, Mazzone S, Iadarola I, Borini A. What criteria for the definition of oocyte quality. *Ann NY Acad Sci* 2004; **144**:132–144.
17. Bradley J, Swann K. Mitochondria and lipid metabolism in mammalian oocytes and early embryos. *Int J Dev Biol* 2019; **63**: 93–103.
18. Collado-Fernandez E, Picton HM, Ré D. Metabolism throughout follicle and oocyte development in mammals. *Int J Dev Biol* 2012; **56**:799–808.
19. Cotterill M, Harris SE, Fernandez EC, Lu J, Huntriss JD, Campbell BK, Picton HM. The activity and copy number of mitochondrial DNA in ovine oocytes throughout oogenesis in vivo and during oocyte maturation in vitro. *Mol Hum Reprod* 2013; **19**: 444–450.
20. Wang LY, Wang DH, Zou XY, Xu CM. Mitochondrial functions on oocytes and preimplantation embryos. *J Zhejiang Univ Sci B* 2009; **10**:483–492.
21. Dumollard R, Carroll J, Duchen MR, Campbell K, Swann K. Mitochondrial function and redox state in mammalian embryos. *Semin Cell Dev Biol* 2009; **20**:346–353.
22. Dumollard R, Campbell K, Halet G, Carroll J, Swann K. Regulation of cytosolic and mitochondrial ATP levels in mouse eggs and zygotes. *Dev Biol* 2008; **316**:431–440.
23. Harris SE, Leese HJ, Gosden RG, Picton HM. Pyruvate and oxygen consumption throughout the growth and development of murine oocytes. *Mol Reprod Dev* 2009; **76**:231–238.
24. Yu Y, Dumollard R, Rossbach A, Lai FA, Swann K. Redistribution of mitochondria leads to bursts of ATP production during spontaneous mouse oocyte maturation. 2010;**316**:672–680.
25. Guérin P, El Mouatassim S, Ménézo Y. Oxidative stress and protection against reactive oxygen species in the pre-implantation embryo and its surroundings. *Hum Reprod Update* 2001; **7**: 175–189.
26. Devine PJ, Perreault SD, Luderer U. Roles of reactive oxygen species and antioxidants in ovarian toxicity. *Biol Reprod* 2012; **86**: 1–10.
27. Walther TC, Farese RV. The life of lipid droplets. *Biochim Biophys Acta Mol Cell Biol Lipids* 2009; **1791**:459–466.
28. Walther TC, Farese RV. Lipid droplets and cellular lipid metabolism. *Annu Rev Biochem* 2012; **81**:687–714.
29. Zhang X, Wang T, Song J, Deng J, Sun Z. Study on follicular fluid metabolomics components at different ages based on lipid metabolism. *Reprod Biol Endocrinol* 2020; **18**:1–8.
30. Dunning KR, Russell DL, Robker RL. Lipids and oocyte developmental competence: the role of fatty acids and β-oxidation. *Reproduction* 2014; **148**:R15–R27.
31. Prates EG, Nunes JT, Pereira RM. A role of lipid metabolism during cumulus-oocyte complex maturation: impact of lipid modulators to improve embryo production. *Mediators Inflamm* 2014: Article ID 692067.
32. Jarc E, Petan T. Lipid droplets and the management of cellular stress. *Yale J Biol Med* 2019; **92**:435–452.
33. Sturmey RG, O'Toole PJ, Leese HJ. Flourescence resonance energy transfer analysis of mitochondrial: lipid association in the porcine oocyte. *Reproduction* 2006; **132**:829–837.
34. Paczkowski M, Schoolcraft WB, Krisher RL. Fatty acid metabolism during maturation affects glucose uptake and is essential to oocyte competence. *Reproduction* 2014; **148**:429–439.
35. Valsangkar D, Downs SM. A requirement for fatty acid oxidation in the hormone-induced meiotic maturation of mouse oocytes. *Biol Reprod* 2013; **89**:1–9.

36. Dunning KR, Akison LK, Russell DL, Norman RJ, Robker RL. Increased Beta-oxidation and improved oocyte developmental competence in response to L-carnitine during ovarian in vitro follicle development in mice. *Biol Reprod* 2011; **85**: 548–555.
37. Dunning KR, Cashman K, Russell DL, Thompson JG, Norman RJ, Robker RL. Beta-oxidation is essential for mouse oocyte developmental competence and early embryo development. *Biol Reprod* 2010; **83**:909–918.
38. Aizawa R, Ibayashi M, Tatsumi T, Yamamoto A, Kokubo T, Miyasaka N, Sato K, Ikeda S, Minami N, Tsukamoto S. Synthesis and maintenance of lipid droplets are essential for mouse preimplantation embryonic development. *Development* 2019; **146**:dev181925.
39. National Research Council. *Guide for the Care and Use of Laboratory Animals*, 8th ed. Washington, DC: National Academes Press; 2011.
40. Hammond L. Measuring cell fluorescence with. *ImageJ* 2014. https://theolb.readthedocs.io/en/latest/imaging/measuring-cell-fluorescence-using-imagej.html.
41. Kasianowicz J, Benz R, McLaughlin S. The kinetic mechanism by which CCCP (carbonyl cyanide m-Chloropheny lhydrazone) transports protons across membranes. *J Membr Biol* 1984; **82**: 179–190.
42. Callicott RJ, Womack JE. Real-time PCR assay for measurement of mouse telomeres. *Comp Med* 2006; **56**:17–22.
43. Pfaffl MW. A new mathematical model for relative quantification in real-time RT-PCR. *Nucleic Acids Res* 2001; **29**:16–21.
44. Matyash V, Liebisch G, Kurzchalia TV, Shevchenko A, Schwudke D. Lipid extraction by methyl-terf-butyl ether for high-throughput lipidomics. *J Lipid Res* 2008; **49**:1137–1146.
45. Pang Z, Chong J, Zhou G de Lima Morais DA, Chang L, Barrette M, Gauthier C, Jacques P-E, Li S, Xia J Metabo analyst 5.0 : narrowing the gap between raw spectra and functional insights. *Nucleic Acids Res* 2021; **49**:388–396.
46. Benkhalifa M, Ferreira YJ, Chahine H, Louanjli N, Miron P, Merviel P, Copin H. Mitochondria: participation to infertility as source of energy and cause of senescence. *Int J Biochem Cell Biol* 2014; **55**:60–64.
47. Liu L, Trimarchi JR, Smith PJS, Keefe DL. Mitochondrial dysfunction leads to telomere attrition and genomic instability. *Aging Cell* 2002; **1**:40–46.
48. Liu L, Trimarchi JR, Navarro P, Blasco MA, Keefe DL. Oxidative stress contributes to arsenic-induced telomere attrition, chromosome instability, and apoptosis. *J Biol Chem* 2003; **278**: 31998–32004.
49. Lopez-Otin C, Blasco MA, Partridge L, Serrano M, Kroemer G. Cell. *Hallmarks Aging* 2013; **153**:1194–1217.
50. Mari M, Morales A, Colell A, Garcia-Ruiz C, Fernandez-Checa JC. Mitochondrial glutathione, a key survival antioxidant. *Antioxid Redox Signal* 2009; **11**:2685–2700.
51. Meyer JN, Leung MCK, Rooney JP, Sendoel A, Hengartner MO, Kisby GE, Bess AS. Mitochondria as a target of environmental toxicants. *Toxicol Sci* 2013; **134**:1–17.
52. Igosheva N, Abramov AY, Poston L, Eckert JJ, Fleming TP, Duchen MR, McConnel JM. Maternal diet-induced obesity alters mitochondrial activity and redox status in mouse oocytes and zygotes. *PLoS One* 2010; **5**:1–8.
53. Pawlak P, Malyszka N, Szczerbal I, Kolodziejski P. Fatty acid induced lipolysis influences embryo development, gene expression and lipid droplet formation in the porcine cumulus cells. *Biol Reprod* 2020; **103**:36–48.
54. Dumollard R, Ward Z, Carroll J, Duchen MR. Regulation of redox metabolism in the mouse oocyte and embryo. *Development* 2007; **134**:455–465.
55. Prasad S, Tiwari M, Pandey AN, Shrivastav TG, Chaube SK. Impact of stress on oocyte quality and reproductive outcome. *J Biomed Sci* 2016; **23**:19–23.
56. Malott K, Luderer U. Toxicant effects on mammalian oocyte mitochondria. *Biol Reprod* 2021; **104**:784–793.
57. Chiaratti MR, Garcia BM, Carvalho KF, Macabelli CH, da Silva Ribeiro FK, Zangiorlamo AF, Sarapiao FD, Seneda MM, Meirelles FV, Guimaraes FEG, Machado TS. Oocyte mitochondria: role on fertility and disease transmission. *Anim Reprod* 2018; **15**:231–238.
58. Wilding M, Dale B, Marino M, di Matteo L, Alviggi C, Pistauro ML, Lombardi L, De Placido G. Mitochondrial aggregation patterns and activity in human oocytes and preimplantation embryos. *Hum Reprod* 2001; **16**:909–917.
59. Willems PHGM, Rossignol R, Dieteren CEJ, Murphy MP, Koopman WJH. Redox homeostasis and mitochondrial dynamics. *Cell Metab* 2015; **22**:207–218.
60. Wai T, Langer T. Mitochondrial dynamics and metabolic regulation. *Trends Endocrinol Metab* 2016; **27**:105–117.
61. Kendig EL, Chen Y, Krishan M, Johansson E, Schneider SN, Genter MB, Nebert DW, Shertzer HG. Lipid metabolism and body composition in Gclm (−/−) mice. *Toxicol Appl Pharmacol* 2011; **257**:338–348.
62. Jamnongjit M, Hammes SR. Oocyte maturation: the coming of age of a germ cell. *Semin Reprod Med* 2005; **23**:234–241.
63. Welte MA. Fat on the move: intracellular motion of lipid droplets. *Biochem Soc Trans* 2009; **37**:991–996.
64. Goodman JM. The gregarious lipid droplet. *J Biol Chem* 2008; **283**:28005–28009.
65. Li L, Zhu S, Shu W, Guo Y, Guan Y, Zeng J, Wang H, Han L, Zhang J, Liu X, Li C, Hou X *et al.* Characterization of metabolic patterns in mouse oocytes during meiotic maturation. *Mol Cell* 2020; **80**:525–540.e9.
66. Prates EG, Nunes JT, Pereira RM. A role of lipid metabolism during cumulus-oocyte complex maturation: impact of lipid modulators to improve embryo production. *Mediators Inflamm* 2014; **2014**: 1–11.
67. Baddela VS, Sharma A, Vanselow J. Non-esterified fatty acids in the ovary: friends or foes? *Reprod Biol Endocrinol* 2020; **18**:1–14. https://doi.org/10.1186/s12958-020-00617-9.
68. Fayezi S, Leroy JLMR, Ghaffari Novin M, Darabi M. Oleic acid in the modulation of oocyte and preimplantation embryo development. *Zygote* 2018; **26**:1–13.
69. Shaaker M, Rahimipour A, Nouri M, Khanaki K, Darabi M, Farzadi L, Shahnazi V, Mehdizadeh A. Fatty acid composition of human follicular fluid phospholipids and fertilization rate in assisted reproductive techniques. *Iran Biomed J* 2012; **16**: 1–7.
70. Wakefield SL, Lane M, Schulz SJ, Hebart ML, Thompson JG, Mitchell M. Maternal supply of omega-3 polyunsaturated fatty acids alter mechanisms involved in oocyte and early embryo development in the mouse. *Am J Physiol Endocrinol Metab* 2008; **294**: 425–434.
71. Mok HJ, Shin H, Lee JW, Lee G-K, Suh CS, Kim KP, Lim HJ. Age-associated lipidome changes in metaphase II mouse oocytes. *PLoS One* 2016; **11**:1–17. https://doi.org/10.1371/journal.pone.0148577.
72. Benador IY, Veliova M, Liesa M, Shirihai OS. Review mitochondria bound to lipid droplets : where mitochondrial dynamics regulate lipid storage and utilization. *Cell Metab* 2019; **29**: 827–835.
73. Benador IY, Veliova M, Mahdaviani K, Petcherski A, Wikstrom JD, Assali EA, Acin-Perez R, Shum M, Oliveira MF, Cinti S, Sztalyrd C, Barshop WD *et al.* Mitochondria bound to lipid droplets have unique bioenergetics, composition, and dynamics that support lipid droplet expansion. *Cell Metab* 2018; **27**:869–885.e6.